An Average Input Current Sensing Method of LLC Resonant Converters for Automatic Burst Mode Control

Jian Chen, *Student Member, IEEE*, Takahide Sato, *Member, IEEE*, Koji Yano, *Member, IEEE*, Hironobu Shiroyama, Makoto Owa, and Masayuki Yamadaya

***Abstract*—Burst mode control techniques have been studied for LLC resonant dc–dc converters to improve power conversion efficiencies at light load conditions. However, there are not many studies about how to detect the load conditions at burst mode not even at normal mode, at the primary side of LLC resonant dc–dc converters. In this paper, we propose and implement a lossless load detection technique for normal and burst modes by a novel average input current sensing method at the primary side of LLC resonant converters. Detailed theoretical analysis at normal and burst modes is presented and a load detection circuit is proposed with the consideration of integrated circuits. To verify the analysis, an LLC resonant offline converter with 400 V input and 16 V/10 A output is simulated using PSIM and a prototype board is built. The experimental results show that the proposed load detection technique is valid and practical. As a result, an automatic burst mode control for LLC resonant converters at light load conditions is realized with the proposed average input current sensing method.**

***Index Terms*—average input current sensing, burst mode, LLC resonant converters, load detection.**

I. Introduction

Due to soft switching techniques and the spread of the anti-capacitive mode protection [1], LLC resonant DC-DC converters are becoming more widely used as the off-line DC-DC converters of televisions, adapters, chargers and LED lightings with power ranges of 100W∼500W. Even though the LLC resonant converters can achieve higher power conversion efficiencies than other PWM topologies at nominal load condition [2], the efficiencies cannot be satisfied at light load conditions, or heavy load conditions with lower output voltages. Recently, there are many studies focused on achieving high efficiency on a wide range of load conditions for LLC resonant converters. Typically, synchronous rectifier techniques are used at heavy load conditions [3], [4], and burst mode control techniques are used at light load conditions [5], [6].

Manuscript received January 24, 2016; revised April 24, 2016; accepted June 6, 2016. Date of publication June 21, 2016; date of current version January 20, 2017. Recommended for publication by Associate Editor Ray-Lee Lin.

J. Chen, H. Shiroyama, M Owa, and M Yamadaya are with the Fuji Electric Co. Ltd., Matsumoto, Nagano 390-0821, Japan (e-mail: ken-chen@fujielectric.com; shiroyama-hironobu@fujielectric.com; owa-makoto@fujielectric.com; yamadaya-masayuki@fujielectric.com).

T. Sato and K Yano are with the University of Yamanashi, Kofu, Yamanashi 400-8510, Japan (e-mail: takahides@yamanashi.ac.jp; yano@yamanashi.ac.jp).

Color versions of one or more of the figures in this paper are available online at http://ieeexplore.ieee.org.

Digital Object Identifier 10.1109/TPEL.2016.2582851

AS for burst mode control techniques at light load conditions, if the load is lighter than a lower predetermined load level, the operation mode of the LLC converters is switched from normal mode to burst mode. On the other hand, if the load is heavier than an upper predetermined load level, it is switched from burst mode to normal mode [7]. In order to realize automatic burst mode control, which is switching operation between normal mode and burst mode automatically, the control systems need to obtain load conditions accurately at both normal mode and burst mode. For off-line converters, detecting the load condition at the primary side is preferred to the secondary side in terms of cost performance. For example, feedback signals that control the pulse widths of power switches are used to reflect the load conditions in pulse width modulation (PWM) control topologies. However, it is difficult for the LLC resonant converters belonging to pulse frequency modulation (PFM) control topologies to reflect the load conditions with the feedback signals that control the switching frequencies. This is because the switching frequencies are almost constant if they are set near the resonant frequency even though the load changes dramatically [8].

For LLC resonant converters with low power, shunt resistors are used to reflect the load conditions at the primary side as expressed in [9]. But shunt resistors cannot be recommended for LLC resonant converters with the nominal power of over 100 W, because the power loss of the shunt resistors is proportional to the nominal power.

In order to detect the load conditions with lossless methods, an input current sensing method is described as [10]. However, it is inaccurate not to consider some parasitic capacitances [11], [12] according the analysis of [10]. A resonant current or voltage sensing method with a lossless network to detect the load conditions is shown in Fig. 1 according to [13], [14]. But it is not suitable for normal mode and especially burst mode at light load conditions since the sensing network works like a divider for the ripple voltage on Cr as described in [13], which has insufficient load dependence. Simulation results of it will be shown in Section IV.

In this paper, we propose a lossless load detection technique for normal and burst mode with a novel average input current sensing method at the primary side of an LLC resonant converter. With the proposed average input current sensing circuit, the load conditions can be obtained accurately at both normal mode and

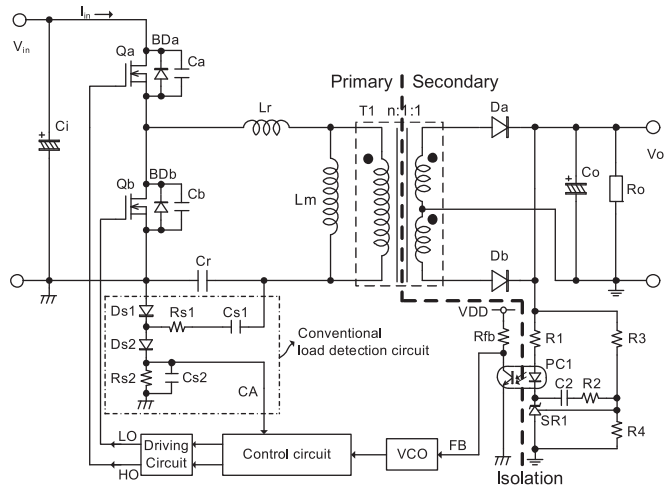

Fig. 1. Circuit diagram of a LLC resonant converter with a conventional load detection circuit.

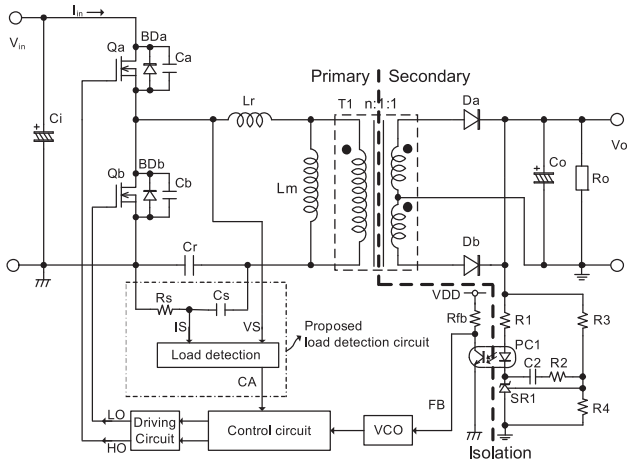

Fig. 2. Circuit diagram of a LLC resonant converter with a proposed load detection circuit by resonant current sensing.

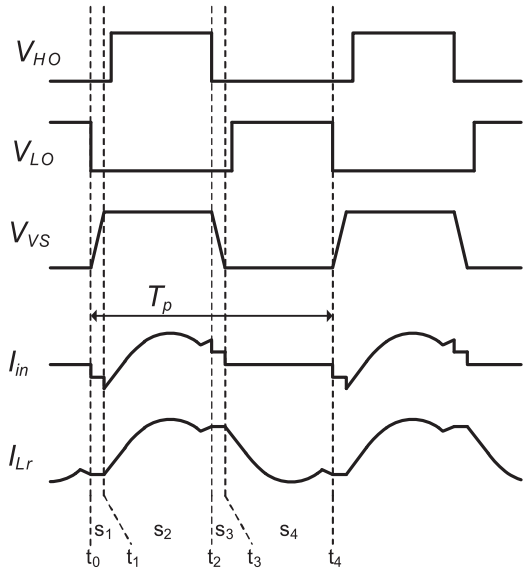

Fig. 3. Typical waveforms of LLC resonant converters.

burst mode. The results of the theoretical analysis are verified by simulation and experiments. An LLC resonant dc–dc converter with 400 V input and 16 V/10 A output is built to show that the load conditions from heavy load to light load can be obtained accurately at the primary side. As a result, an automatic burst mode control is realized for the LLC resonant converter with the proposed lossless load detection technique.

II. Improved LLC Resonant Converters

An LLC resonant dc–dc converter with isolation between the primary side and the secondary side is shown in Fig. 2.

In the main power circuit, there are a high-side part and a low-side part at the primary side. At the high-side part, there are a power MOSFET Qa with a body-diode BDa, and a capacitor Ca with the output capacitance of Qa and extra capacitance if required. In the low-side part, there are Qb, BDb, and Cb same as the high-side part, and a resonant tank including resonant inductor Lr, magnetizing inductor Lm and resonant capacitor Cr. There is an ideal transformer T1 with a center-tapped structure by which energy is transferred from the primary side to the secondary side with isolation. Generally, Lr, Lm, and T1 are integrated into one transformer [8], [15], [16]. At the secondary side, there are two rectifier diodes Da and Db, a rectifier capacitor Co, and the output resistor Ro called as load.

In the control circuits of the primary side, the control units are integrated into one control IC, except some big capacitors, etc. There are a driving circuit, a control circuit unit, a voltage-controlled oscillator VCO, and the proposed load detection circuit with two input signals and one output signal. One input signal of the load detection circuit is a voltage level $V_{\rm IS}$, which reflects the resonant current $(I_{\rm Lr})$ through a current divider Cs and Rs, which is called the "lossless" sensing technique with a capacitive shunt [17]. The other one is a voltage level V_{VS}, which is the drain voltage of the low-side power MOSFET Qb. It is noted that the V_{VS} is approximately detected by an auxiliary winding at the primary side of the transformer when implementing the experiment to simplify the control IC. The output signal of the load detection circuit is a voltage level V_{CA}, which reflects the load conditions. The unit of control circuit determines the operation mode such as normal and burst modes at light load conditions according to V_{CA} by comparing with predetermined levels.

The isolation of the control circuit between the primary side and the secondary side is implemented by a photo-coupler PC1, a shunt regulator SR1, and phase compensation parts R1, C2, and R2, etc.

III. Analysis and Design

In this section, detailed theoretical analysis at normal and burst modes is presented and a load detection circuit is proposed with the consideration of integrated circuits (ICs).

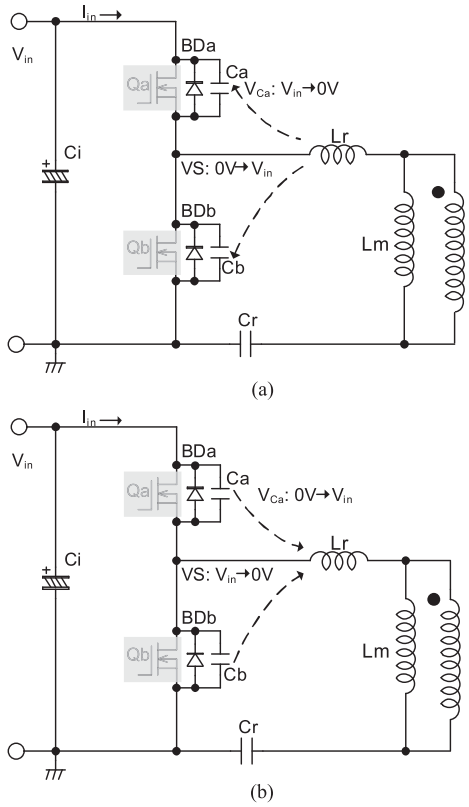

Fig. 4. (a) Transition state s1 with discharge of Ca. (b) Transition state s3 with charge of Ca.

A. Normal Mode Operation

Typical operation waveforms (discontinuous conduction mode) of the LLC resonant converters at normal mode are shown in Fig. 3 [18], [19]. Generally, the output power can be expressed as (1) for periodic switching operation

$$P_o = \eta \cdot P_{\rm in} = \eta \cdot V_{\rm in} \cdot \frac{1}{T_p} \cdot \int_0^{T_p} I_{\rm in}(t)\, dt \tag{1}$$

where $P_{\rm in}$ is the input power of the LLC resonant converter, P_o is the output power, η is the power conversion efficiency, $V_{\rm in}$ is the input dc voltage with a constant value, T_p is the switching period of the resonant operation, and $I_{\rm in}(t)$ is the input current, which is a function of time.

The input current $I_{\rm in}(t)$ can be separated into four operation states as shown in Fig. 3. According to (1), the output power can be expressed as

$$\begin{aligned} P_o = \eta \cdot V_{\rm in} \cdot \tfrac{1}{T_p} \cdot \left(\int_{t_0}^{t_1} I_{\rm is_1}(t)\, dt + \int_{t_1}^{t_2} I_{\rm is_2}(t)\, dt \right. \\ \left. + \int_{t_2}^{t_3} I_{\rm is_3}(t)\, dt + \int_{t_3}^{t_4} I_{\rm is_4}(t)\, dt\right) \end{aligned} \tag{2}$$

where $I_{\rm is1}(t), I_{\rm is2}(t), I_{\rm is3}(t)$, and $I_{\rm is4}(t)$ stand for the input current at the states of s_1, s_2, s_3, and s_4, respectively.

The states of s_1 and s_3 are the transition states with the charge or discharge of Ca, Cb, and other parasitic capacitances by the current flowing through Lr as shown in Fig. 4. In this paper, the parasitic capacitances [11], [12] are ignored since they have no effect on the analysis of the proposed load detection technique.

At the transition state s_1, Ca is discharged by the part of the resonant current I_{Lr}, which is equal to the input current $I_{\rm in}$, and the voltage of Ca ($V_{\rm Ca}$) is discharged from V_{in} to 0. At the transition state s_3, Ca is charged by the part of resonant current I_{Lr}, which is equal to the input current $I_{\rm in}$ too, and V_{Ca} is changed from 0 to $V_{\rm in}$. Accordingly, the integration of the input current at the state s_1 and s_3 of (2) can be given by (3) and (4), respectively

$$\int_{t_0}^{t_1} I_{\rm is_1}(t)\, dt = -V_{\rm in} \cdot Ca \tag{3}$$

$$\int_{t_2}^{t_3} I_{\rm is_3}(t)\, dt = V_{\rm in} \cdot Ca. \tag{4}$$

As for the state s_2, it is the resonant state where the input current $I_{\rm in}(t)$ is equal to the resonant current $I_{Lr}(t)$. Therefore, the integration of input current at the state of s_2 of (2) can be expressed as

$$\int_{t_1}^{t_2} I_{\rm is_2}(t)\, dt = \int_{t_1}^{t_2} I_{Lr}(t)\, dt. \tag{5}$$

As for the state s_4, since $I_{\rm is4}(t)$ is zero, the integration of input current at the state of s_4 of (2) can be expressed simply as

$$\int_{t_3}^{t_4} I_{is_4}(t)\, dt = 0. \tag{6}$$

By substituting (3)–(6) into (2), the output power can be obtained as

$$P_o = \eta \cdot V_{\rm in} \cdot \frac{1}{T_p} \cdot \int_{t_1}^{t_2} I_{Lr}(t)\, dt. \tag{7}$$

It can be seen that the output power is directly proportional to the mean value of the resonant current during the state s_2 with period T_p. Since t_1 is the end timing of VS rising and t_2 is the start timing of VS falling, as shown in Fig. 3, the output power can be obtained by detecting the resonant current $I_{Lr}(t)$ and the timing of VS voltage V_{VS}.

The resonant current $I_{Lr}(t)$ can be detected by a current divider Cs and then transferred into a voltage level $V_{\rm IS}(t)$ with a resistor Rs as shown in Fig. 2. With the first harmonic approximation [20]–[22] of the resonant current $I_{Lr(t)}, V_{\rm IS(t)}$ can be expressed as

$$V_{\rm IS}(t) = I_{Lr}(t) \cdot \left| \frac{R_s \cdot (1 + \frac{Cr}{Cs}) - j \cdot 2 \cdot \pi \cdot f_s \cdot Rs^2 \cdot Cr}{(1 + \frac{Cr}{Cs})^2 + (2 \cdot \pi \cdot f_s \cdot Rs \cdot Cr)^2} \right| \tag{8}$$

where f_s is the frequency of the resonant current $I_{Lr}(t)$.

And the phase shift ($\theta_{\rm VIS}$) of $V_{\rm IS}(t)$ against $I_{Lr}(t)$ can be expressed as

$$\tan(\theta_{\rm VIS}) = -\frac{2 \cdot \pi \cdot f_s \cdot Rs \cdot Cr \cdot Cs}{Cs + Cr}. \tag{9}$$

According to the practical parameters listed in Table I, the parts with f_s at (8) are much smaller than other parts without f_s, and can be ignored approximately. Therefore, $V_{\rm IS}(t)$ can be expressed simply as

$$V_{\rm IS}(t) = I_{Lr}(t) \cdot \frac{Rs \cdot Cs}{(Cs + Cr)}. \tag{10}$$

TABLE I
PRACTICAL PARAMETERS FOR THE CURRENT DIVIDER CIRCUIT

Symbol	Designed parameters	Parameter value
Rs	Resistance of current divider	220 Ω
Cs	Capacitance of current divider	220 pF
Cr	Resonant capacitor	22 nF
f_s	Operating frequency	78 kHz∼84 kHz

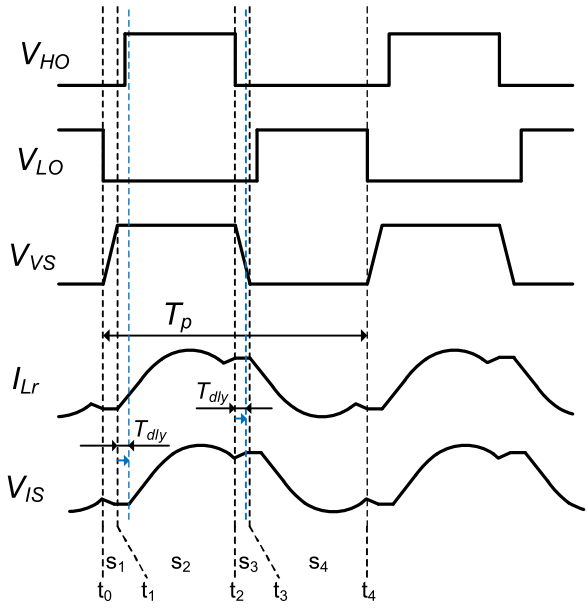

Fig. 5. Waveforms of V_{HO}, V_{LO}, V_{VS}, I_{Lr} and $V_{\rm IS}$.

It is noted that even the operating frequency is up to 500 kHz, the tolerance of (10) compared with (8) is only 1.1%. It is because the fs parts appear at both numerator and denominator in (8).

According to (9), the propagation delay T_{dly} from $I_{Lr}(t)$ to $V_{\rm IS}(t)$, as shown in Fig. 5, can be expressed approximately as

$$T_{dly} = \frac{Rs \cdot Cs \cdot Cr}{(Cs + Cr)} \tag{11}$$

Here, $\tan(\theta_{VIS}) \approx \theta_{VIS}$ and $|\theta_{VIS}| = 2 \cdot \pi \cdot f_s \cdot T_{dly}$ are used.

Consequently, the output power can be deduced as

$$P_o = \eta \cdot V_{\rm in} \cdot \frac{Cs + Cr}{Rs \cdot Cs} \cdot \frac{1}{T_p} \cdot \int_{t_1+T_{dly}}^{t_2+T_{dly}} V_{\rm IS}(t)\, dt. \tag{12}$$

The mean value of $V_{\rm IS}(t)$ at the state of s_2 with propagation delay of T_{dly} during period T_p can be obtained by a proposed circuit as shown in Fig. 6. The transition timing of *VS* is detected by a hysteresis comparator with reference voltages of $V_{\rm ref1}/V_{\rm ref2}$ which are set close to $V_{\rm in} \cdot R_{VS2}/(R_{VS1} + R_{VS2})$.

At the end timing of VS rising with delay of T_{dly}, SW_1 turns ON and SW_2 turns OFF, so IS voltage $(V_{\rm IS})$ becomes the input voltage of the RC filter. At the start timing of VS falling with delay of T_{dly}, SW_1 turns off and SW_2 turns on, so zero voltage

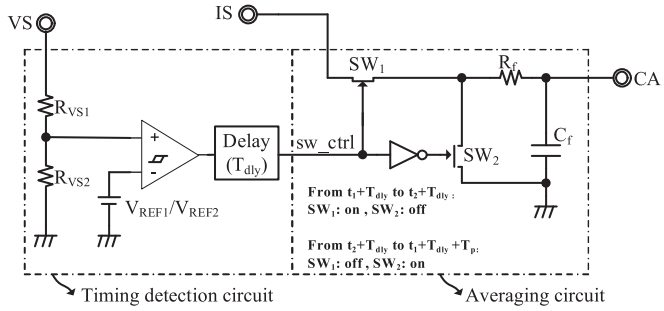

Fig. 6. Proposed circuit diagram of the load detection.

becomes the input voltage of the RC filter. Therefore, the voltage of CA $(V_{\rm CA})$ can be expressed as

$$V_{CA} = \frac{1}{T_p} \cdot \int_{t_1+T_{dly}}^{t_2+T_{dly}} V_{IS}(t)\, dt. \tag{13}$$

Here, it is assumed that the time constant of the RC filter ($R_{\rm f}$ and $C_{\rm f}$ in Fig. 6) is much larger than T_p.

By substituting (13) into (12), the output power is directly proportional to V_{CA}, as shown in (14). In other words, we can achieve the load conditions at the primary side by the values of V_{CA}

$$P_o = \eta \cdot V_{\rm in} \cdot \frac{Cs + Cr}{Rs \cdot Cs} \cdot V_{CA}. \tag{14}$$

It is noted that the results are completely applicable to the continuous conduction mode of LLC resonant converters as well by following the same derivation procedure.

B. Burst Mode Operation

In this paper, we present a kind of burst mode whose burst frequency is more than 20 kHz to avoid audible noise. The purpose of it is to improve efficiencies at light load below around 20% nominal load. It should be noted that it is difficult to get high efficiency performance for this kind of burst mode at very light load condition due to the limitation of the burst frequency.

The presented burst mode is shown in Fig. 7, where the input current consists of three regions. The first region is the switching region at T_{pb1}, the second region is the circulating region at T_{pb2}, and the third one is the resonant region at T_{pb3} with the resonant frequency of f_c as

$$f_c = \frac{1}{2 \cdot \pi \cdot \sqrt{(Lm + Lr) \cdot \frac{(Ca+Cb) \cdot Cr}{Ca+Cb+Cr}}}. \tag{15}$$

It is noted that the start of each burst is determined by VCO and VS voltages, and the stop of each burst is controlled by VCO. The width of the cycles at the first region is different from each other.

At burst mode, similar to the analysis of normal mode, the output power can be expressed as

$$P_o = \eta \cdot V_{\rm in} \cdot \tfrac{1}{T_{pb}} \cdot \left(\int_{t_{14}}^{t_8} I_{ipb_1}(t)\, dt + \int_{t_8}^{t_{12}} I_{ipb_2}(t)\, dt + \int_{t_{12}}^{t_{13}} I_{ipb_3}(t)\, dt\right) \tag{16}$$

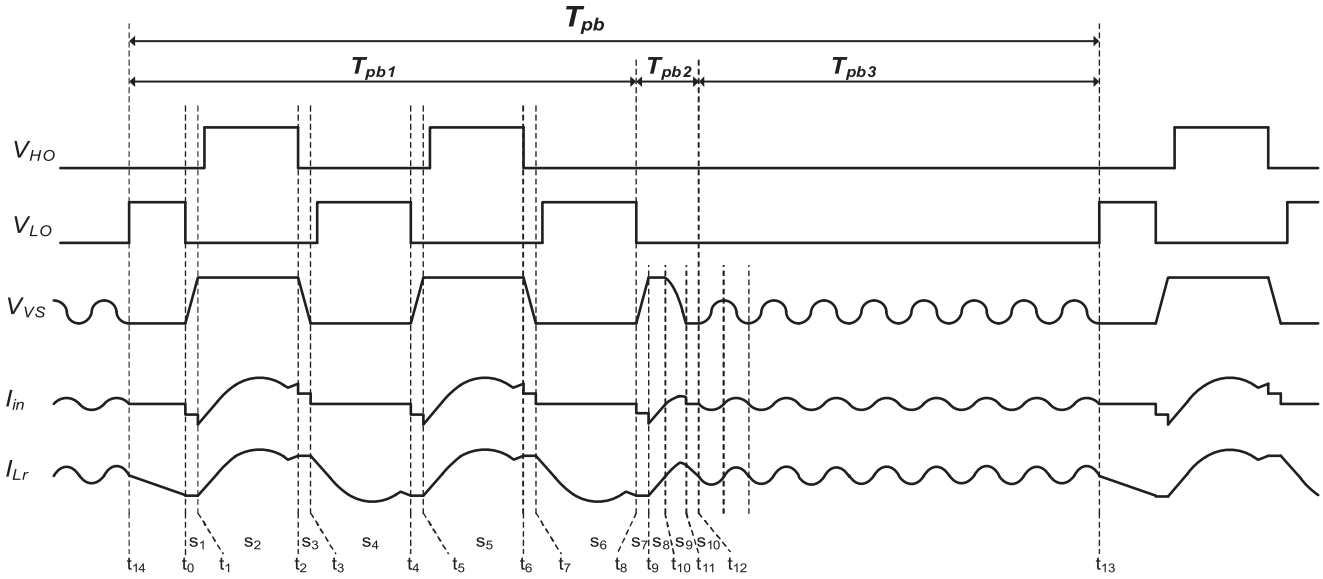

Fig. 7. Typical waveforms of LLC resonant converters at burst mode.

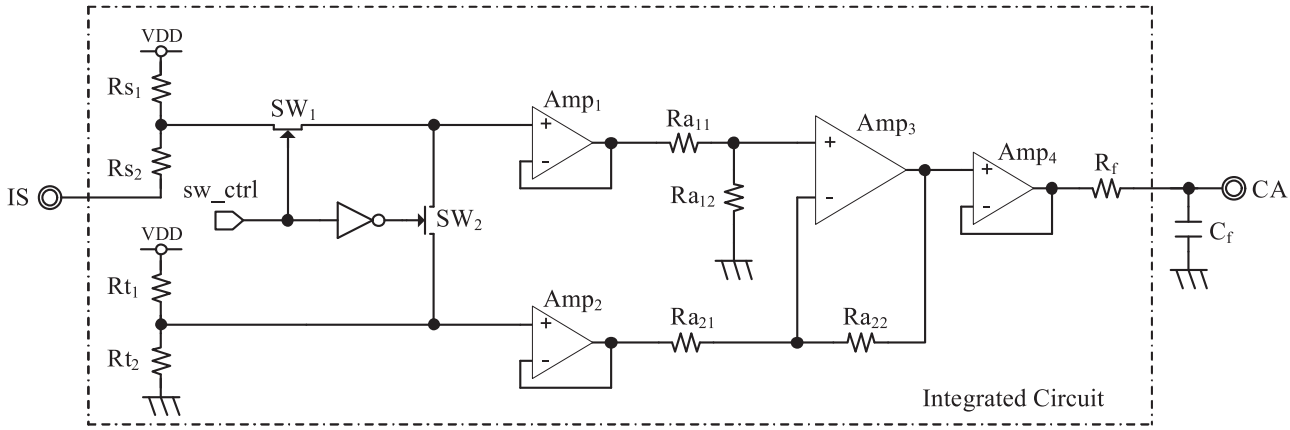

Fig. 8. Proposed circuit diagram of the averaging circuit with IC.

where T_{pb} is the burst period.

The first integration of (16) can be given by

$$\int_{t_{14}}^{t_8} I_{ipb_1}(t)\,dt = \int_{t_1}^{t_2} I_{\mathrm{is}_2}(t)\,dt + \int_{t_5}^{t_6} I_{\mathrm{is}5}(t)\,dt. \tag{17}$$

On the other hand, the second integration of (16) can be obtained as

$$\begin{aligned}\int_{t_8}^{t_{12}} I_{ipb_2}(t)\,dt = {} & \int_{t_8}^{t_9} I_{\mathrm{is}_7}(t)\,dt + \int_{t_9}^{t_{10}} I_{\mathrm{is}_8}(t)\,dt \\ & + \int_{t_{10}}^{t_{11}} I_{\mathrm{is}_9}(t)\,dt + \int_{t_{11}}^{t_{12}} I_{\mathrm{is}10}(t)\,dt.\end{aligned} \tag{18}$$

At the transition state s_9, Ca is charged by the part of resonant current due to the resonant operation with resonant frequency f_c. As a result, the voltage of Ca (V_{Ca}) is changed from 0 to V_{in}. Therefore, (19) can be obtained

$$\int_{t_{10}}^{t_{11}} I_{\mathrm{is}_9}(t)\,dt = V_{\mathrm{in}} \cdot Ca. \tag{19}$$

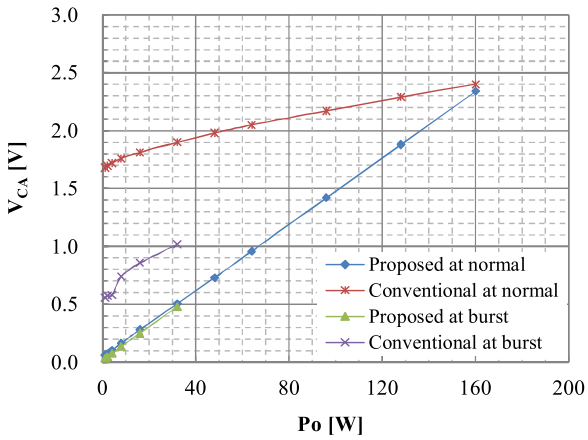

Fig. 9. V_{CA} level against output power P_o at normal and burst mode with proposed load detection technique, compared with conventional based on simulation.

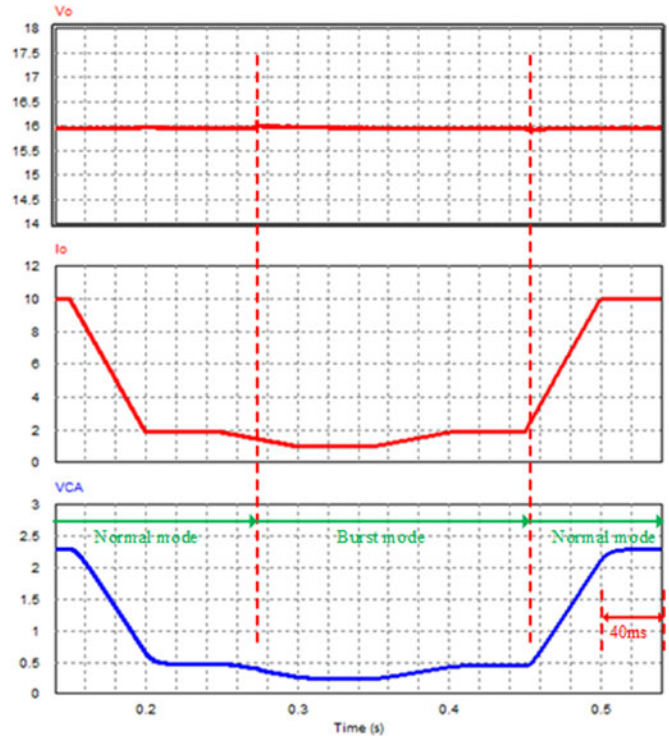

Fig. 10. Simulated waveforms V_O, I_O and V_{CA}, based on parameters listed in Table II for the proposed technique.

Similar to the analysis of normal mode, the second integration of (16) can be obtained as

$$\int_{t_8}^{t_{12}} I_{ipb_2}(t)\,dt = \int_{t_9}^{t_{10}} I_{\mathrm{is}_8}(t)\,dt. \tag{20}$$

Regarding the third integration of (16), since it is a complete resonant operation with resonant frequency f_c, as expressed in (15), it is clear that the result of the third integration of (16) is zero.

Consequently, the output power at burst mode can be expressed as

$$P_o = \eta \cdot V_{\mathrm{in}} \cdot \tfrac{1}{T_{pb}} \cdot \left(\int_{t_1}^{t_2} I_{\mathrm{is}_2}(t)\,dt + \int_{t_5}^{t_6} I_{\mathrm{is}_5}(t)\,dt + \int_{t_9}^{t_{10}} I_{\mathrm{is}_8}(t)\,dt\right). \tag{21}$$

Similar to the analysis of normal mode, the output power at burst mode can be expressed as

$$P_o = \eta \cdot V_{\mathrm{in}} \cdot \tfrac{Cs+Cr}{Rs\cdot Cs} \cdot \tfrac{1}{T_{pb}} \cdot \left(\int_{t_1+T_{dly}}^{t_2+T_{dly}} V_{is}(t)\,dt + \int_{t_5+T_{dly}}^{t_6+T_{dly}} V_{\mathrm{is}}(t)\,dt + \int_{t_9+T_{dly}}^{t_{10}+T_{dly}} V_{\mathrm{is}}(t)\,dt\right). \tag{22}$$

Since t_1, t_5, and t_9 are the end timings of VS rising, and t_2, t_6, and t_{10} are the start timings of VS falling, the proposed circuit as shown in Fig. 6 is valid same as normal mode. The voltage of CA (V_{CA}) at burst mode can be expressed as

$$V_{CA} = \tfrac{1}{T_{pb}} \cdot \left(\int_{t_1+T_{dly}}^{t_2+T_{dly}} V_{is}(t)\,dt + \int_{t_5+T_{dly}}^{t_6+T_{dly}} V_{is}(t)\,dt + \int_{t_9+T_{dly}}^{t_{10}+T_{dly}} V_{is}(t)\,dt\right). \tag{23}$$

Here, it is assumed that the time constant of an RC filter (R_{f} and C_{f} in Fig. 6) is much larger than T_{pb}.

As a result, (14) is valid for both normal mode and burst mode. In other words, the load conditions can be detected by the voltage levels of CA (V_{CA}) regardless of the operation modes.

It is clear that the derivation process from (16) to (23) is applicable to any burst mode operations of LLC resonant converters theoretically.

C. Consideration of ICs

Regarding the averaging circuit of Fig. 6, it is not easy to integrate the SW_1 and SW_2 into a control IC since V_{IS} has a minus voltage part. Accordingly, a circuit with level shift circuits, which is available to be integrated into a control IC, is proposed as shown in Fig. 8. The capacitor C_{f} is connected to the terminal CA of the control IC to adjust the time constant of the RC filter. It is noted that, in order to get a stable control on the averaging circuit, the signal sw_ctrl is set as low by the control system at the resonant part T_{pb3} in Fig. 7.

When SW_1 is on, the DC gain k_{CA} between CA and IS can be given as

$$k_{CA} = \frac{V_{CA}}{V_{IS}} = \frac{Rs_1}{Rs_1 + Rs_2} \cdot \frac{Ra_{12}}{Ra_{11}}. \tag{24}$$

Here it is assumed that

$$\frac{Rs_1}{Rs_2} = \frac{Rt_1}{Rt_2}, \frac{Ra_{12}}{Rt_2} = \frac{Ra_{22}}{Ra_{21}}.$$

Therefore, (13) can be modified as

$$\frac{V_{CA}}{k_{CA}} = \frac{1}{T_p} \cdot \int_{t_1+T_{dly}}^{t_2+T_{dly}} V_{IS}(t)\,dt. \tag{25}$$

As a result, the linear relationship of P_o and V_{CA} can be obtained as (26) by modifying (14)

$$P_o = \eta \cdot V_{in} \cdot \frac{Cs + Cr}{Rs \cdot Cs} \cdot \frac{V_{CA}}{k_{CA}}. \tag{26}$$

According to the (26), the dc gain k_{CA} can compensate the change of V_{in} by making V_{in}/k_{CA} as a constant. For example, the resistance of Ra_{12} and Ra_{22} can be controlled by using the value of V_{in} in the control IC. For the sake of simplicity, V_{in} and k_{CA} are set as a constant value 400 V and 2.5 at the following sections.

From the (26), it can be seen that η has effect on the linear relationship of P_o and V_{CA} due to the P_o dependence or operation mode dependence of η. But in terms of auto burst mode control, the change of η at the load points of mode switching will not impact the load detection accuracy, because we always try to set the load points of mode switching to reduce the change of η as small as possible such as 2% or less.

Additionally, in the (26), since there are no any parameters such as operating frequency, parasitic capacitances in the resonant tank and so on. It is clear that the proposed load detection method is not only accurate but insensitive to the statistical spread of the components of the resonant tank in mass production.

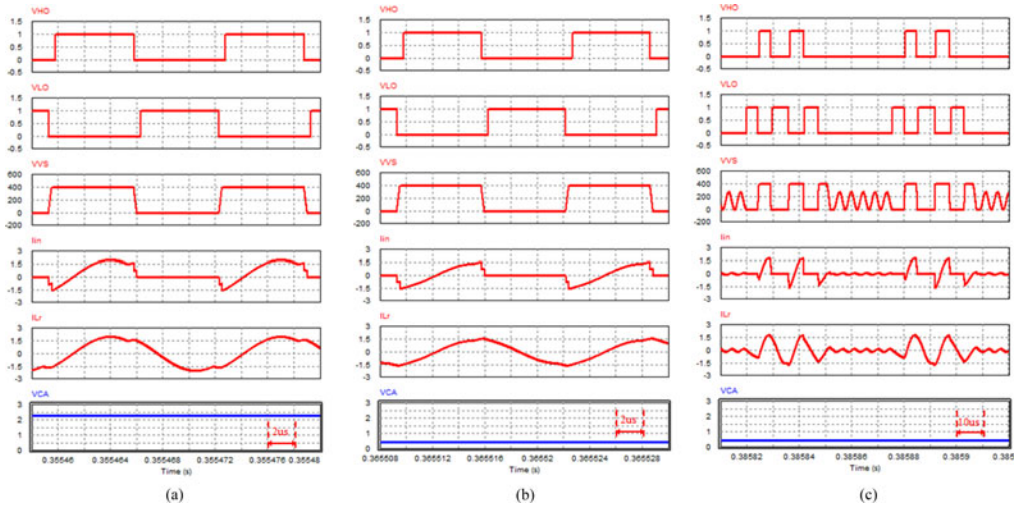

Fig. 11. Simulated waveforms based on parameters listed in Table II for the proposed technique. (a) Normal mode at nominal load ($P_o = 160$ W). (b) Normal mode at light load ($P_o = 30$ W). (c) Burst mode at light load ($P_o = 30$ W).

TABLE II
PARAMETERS FOR PROPOSED AND CONVENTIONAL TECHNIQUES

Symbol	Designed parameters	Parameter value	
		Proposed	Conventional
V_{in}	Input voltage	400 V	
V_o	Output voltage	16 V	
Lo	Inductance of primary winding with secondary winding open	568 uH	
Ls	Inductance of primary winding with secondary winding short	150 uH	
N	Turns ratio	48:3:3	
Cr	Resonant capacitance	22 nF	
Ron	On resistance of Qa or Qb	0.49 Ω	
Ca	Capacitance of Ca	470 pF	
Cb	Capacitance of Cb	470 pF	
V_F	Forward voltage of Da or Db	0.5 V	
Cs	Capacitance of current divider	220 pF	-
Rs	Resistance of current divider	220 Ω	-
T_{dly}	Propagation delay for VS timing detection	48 ns	-
k_{CA}	The DC gain of CA against IS	2.5	-
R_f	Resistance of R_f	100 kΩ	-
C_f	Capacitance of C_f	0.1 uF	-
Cs_1	Capacitance of Cs_1	-	220 pF
Rs_1	Resistance of Rs_1	-	10 kΩ
Cs_2	Capacitance of Cs_2	-	4.7 uF
Rs_2	Resistance of Rs_2	-	560 Ω

IV. SIMULATION RESULTS

Fig. 9 shows the curve of the load condition V_{CA} against output power P_o with the proposed load detection technique, compared with the conventional technique whose circuit diagram is shown in Fig. 1.

The simulation is implemented using PSIM with parameters listed in Table II for the proposed technique and the conventional techniques [13]. It is noted that the transformer model is built based on the integrated transformers, which use inductance parameters of the primary winding with the secondary winding open or short [22].

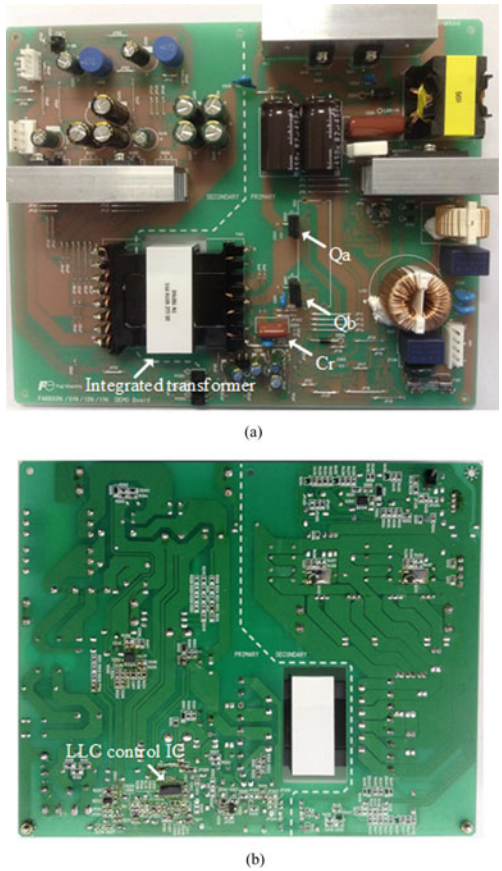

Fig. 12. Evaluation board. (a) Power circuits. (b) Control circuits with a LLC-IC for the LLC resonant converter.

It can be seen that V_{CA} can reflect the load condition well not only at normal mode but burst mode. On the other hand, with the conventional technique, it is clear that the curves of the load conditions between normal and burst modes have such a big difference that it is not suitable for automatic burst mode control.

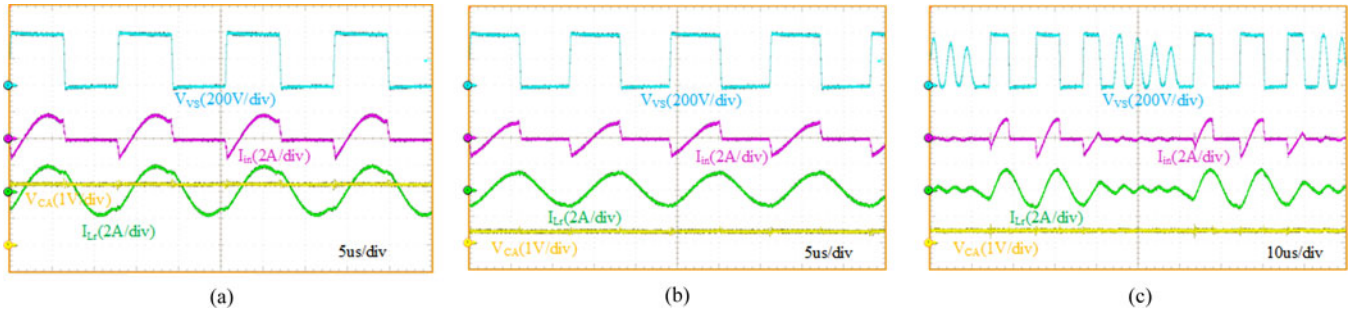

Fig. 13. Experimental waveforms. (a) Nominal load ($\mathrm{P_o} = 160$ W) at normal mode. (b) Light load ($\mathrm{P_o} = 30$ W) at normal mode. (c) Light load ($\mathrm{P_o} = 30$ W) at burst mode.

TABLE III
PARAMETERS OR DEVICES FOR EXPERIMENTAL TEST

Symbol	Designed parameters	Parameter value
V_{in}	Input voltage	400 V
V_o	Output voltage	16 V
Lo	Inductance of primary winding with secondary winding open	568 uH
Ls	Inductance of primary winding with secondary winding short	150 uH
N	Turns ratio	48:3:3
Cr	Resonant capacitance	22 nF
Qa, Qb	Power mosfets	FMV07N60S1
Ca	Extra capacitance of Ca	220 pF
Cb	Extra capacitance of Cb	220 pF
Da, Db	Rectifier diodes	YG862C04R
Cs	Capacitance of current divider	220 pF
Rs	Resistance of current divider	220 Ω
k_{CA}	The DC gain of CA against IS	2.5
R_f	Resistance of $\mathrm{R_f}$	100 kΩ
C_f	Capacitance of $\mathrm{C_f}$	0.1 uF

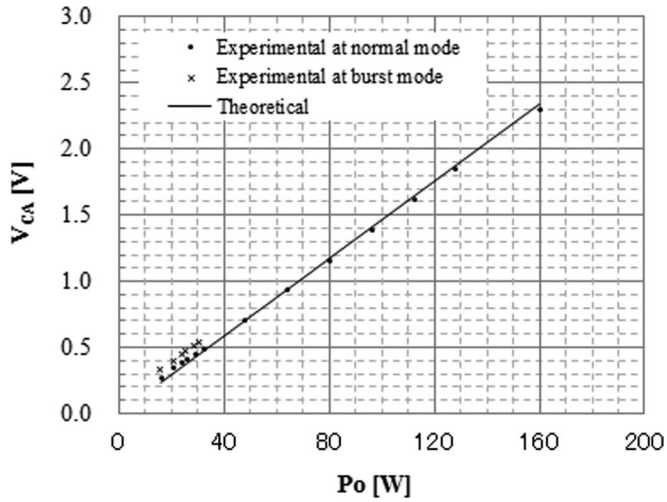

Fig. 14. V_{CA} level against output power P_{o} at normal and burst mode with comparison to theoretical results.

Fig. 10 shows the waveforms of V_O, I_O and V_{CA} from heavy load to light load, and then back to heavy load with automatic burst mode control by the proposed techniques. When V_{CA} is lower than one predetermined level (0.4 V), the converter enters burst modest mode. And then when V_{CA} is higher than another predetermined level (0.5 V), it leaves burst mode. It is noted that the predetermined levels of V_{CA} are set to reduce the change of the power efficiencies as small as possible when the operation mode is switched.

Fig. 11 shows three points of Fig. 10 with detailed waveforms, $V_{HO}, V_{LO}, V_{VS}, I_{\mathrm{in}}, I_{Lr}$ and V_{CA} at the heavy load of 160 W ($\mathrm{I_o} = 10$ A) at normal mode, and a light load of 30 W ($\mathrm{I_o} = 1.875$ A) operating at normal mode and burst mode.

In order to obtain the accurate data of V_{CA} levels at burst mode, the time constant of R_{f} and C_{f} is set as 10 ms, which impacts clearly the load response from light load to nominal load condition at burst mode, because it takes time to leave the burst mode, which cannot provide the nominal power. But it is possible to improve the load response by adding an RC filter before the route of R_{f} and C_{f} in Fig. 8. The new RC filter is built with a short time constant such as 0.5 ms or less in the control IC and the output voltage of it is used to leave the burst mode rapidly at the transition load condition. We will implement the improvement method of the load response in future work.

V. EXPERIMENTAL RESULTS

A prototype of the LLC resonant converter is built by modifying the evaluation board of Fuji Electric, as shown in Fig. 12, where the line filter and the PFC converter are not used. Its input voltage is 400 V and output voltage is 16 V with a nominal power of 160 W ($\mathrm{I_o} = 10$ A). The parameters or devices for this experimental test are listed in Table III. A prototype of the LLC control IC is used, which is the next generation of FA6A00N series described in [23].

Fig. 13 shows the experimental waveforms of $V_{VS}, I_{\mathrm{in}}, I_{Lr}$ and V_{CA} at the nominal load of 160 W at normal mode, and a light load of 30 W operating at normal mode and burst mode. It can be seen that the experimental results of load condition V_{CA} meet simulation results very well.

Fig. 14 illustrates the curves of V_{CA} against P_{o} with theoretical and experimental results. The theoretical results are calculated by (26) where the efficiency is set as a constant value of 0.93 based on the experimental data at the nominal load condition. It is confirmed that the experimental results meet the theoretical results from heavy load to light load well. It should be noted that if the theoretical results take the P_o dependence of η into account, it will meet the experimental results better. As for auto burst mode control, the predetermined levels of V_{CA} for

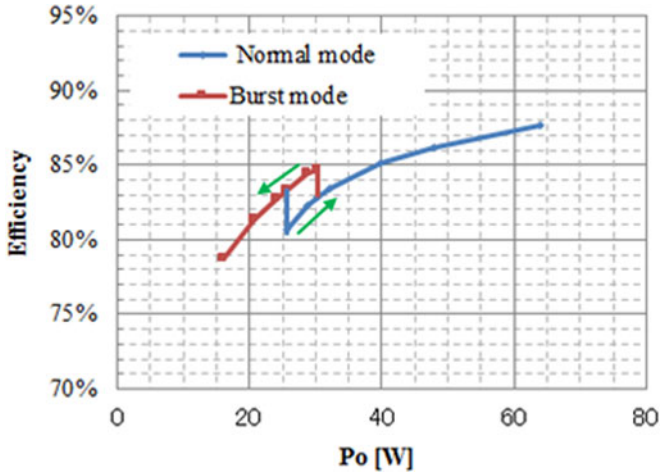

Fig. 15. Experimental efficiency at light load with automatic burst mode control.

entering or leaving burst mode are selectable by the control IC. The predetermined levels of V_{CA} are determined by reducing the change of power efficiencies as small as possible when the operation mode is switched. In this paper, the predetermined levels of V_{CA} are selected as 0.4 and 0.5 V.

Fig. 15 shows the experimental efficiencies at light load with automatic burst mode control. When the load decreases under 24 W, the switching operation is switched to burst mode from normal mode. When the load increases to 30 W, the switching operation is back to normal mode. It can be seen that the efficiencies at burst mode are higher than that at normal mode. As a result, an automatic burst mode control that improves the efficiencies at light load for LLC resonant converter is realized experimentally.

VI. Conclusion

In this paper, for LLC resonant converters, a lossless load detection technique for normal and burst modes by a novel average input current sensing method is presented. Based on the theoretical analysis on normal and burst modes, a load detection circuit is proposed with consideration of ICs. To verify the theoretical analysis and proposed circuits, an LLC resonant converter with 400 V input and 16 V/10 A output is simulated with PSIM and a prototype board is built. The simulation and experimental results show that the proposed load detection technique is valid and practical. As a result, an automatic burst mode control for the LLC resonant converters is realized to achieve higher efficiency at light load conditions. In future work, we will implement the improvement method of the load response.

References

[1] "12 V - 150 W resonant converter with synchronous rectification using the L6563H, L6699 and SRK2000A AN4027, [Online]. Available: www.st.com

[2] B. Yang, F. Lee, A. Zhang, and G. Hua, "LLC resonant converter for front end dc/dc conversion," in *Proc. IEEE 17th Annu. Conf. Appl. Power Electron. Expo.*, Mar. 2002, pp. 1108–1112.

[3] D. Fu, Y. Liu, and F. Lee, "A novel driving scheme for synchronous rectifiers in LLC resonant converters," *IEEE Trans. Power Electron.*, vol. 24, no. 5, pp. 1321–1329, May 2009.

[4] J. Zhang, J. Liao, J. Wang, and Z. Qian, "A current-driving synchronous rectifier for an llc resonant converter with voltage-doubler rectifier structure," *IEEE Trans. Power Electron.*, vol. 27, no. 4, pp. 1894–1904, Apr. 2012.

[5] W. Feng, F. Lee, and P. Mattavelli, "Optimal trajectory control of burst mode for *LLC* resonant converter," *IEEE Trans. Power Electron.*, vol. 28, no. 1, pp. 457–466, Jan. 2013.

[6] S. Zhao, J. Xu, and O. Trescases, "Burst-mode resonant llc converter for an led luminaire with integrated visible light communication for smart buildings," *IEEE Trans. Power Electron.*, vol. 29, no. 8, pp. 4392–4402, Aug. 2014.

[7] B. Wang, X. Xin, S. Wu, H. Wu, and J. Ying, "Analysis and implementation of llc burst mode for light load efficiency improvement," in *Proc. IEEE 24th Annu. Conf Appl. Power Electron. Expo.*, Feb. 2009, pp. 58–64.

[8] H. Choi, "Analysis and design of LLC resonant converter with integrated transformer," in *Proc. IEEE 22nd Annu. Conf. Appl. Power Electron. Expo.*, Feb. 2007, pp. 1630–1635.

[9] Y. Fang, D. Xu, Y. Zhang, F. Gao, L. Zhu, and Y. Chen, "Standby mode control circuit design of LLC resonant converter," in *Proc. IEEE Int. Conf. Power Electron. Spec.*, Jun. 2007, pp. 726–730.

[10] Z. Hu, Y. Liu, and P. Sen, "Cycle-by-cycle average input current sensing method for LLC resonant topologies," in *Proc. IEEE Int. Conf. Energy Conv. Congr. Expo.*, Sep. 2013, pp. 167–174.

[11] Z. Hu, Y. Liu, and P. Sen, "Analysis of LLC resonant converter considering effects of parasitic components," in *Proc. IEEE Int. Conf. Telecommun. Energy*, Oct. 2009, pp. 1–6.

[12] "Half bridge resonant LLC converters and primary side MOSFET selection," AN4720, [Online]. Available: www.st.com

[13] "Application Note for an LLC Resonant Converter Using Resonant Controller HR1000", AN054, [Online]. Available: www.MonolithicPower.com

[14] "L6598 off-line controller for Resonant Converters", AN1673, [Online], Available: www.st.com

[15] S. Yang, S. Abe, and M. Shoyama, "Design consideration of flat transformer in LLC resonant converter for low core loss," in *Proc. IEEE Int. Conf. Power Electron.*, Jun. 2010, pp. 1630–1635.

[16] C. Adragna, S. De Simone, and C. Spini, "A design methodology for LLC resonant converters based on inspection of resonant tank currents," in *Proc. IEEE 23rd Annu. Conf. Appl. Power Electron. Expo.*, Feb. 2008. pp. 1361–1367.

[17] L6699 Enhanced high voltage resonant controller, [Online]. Available: www.st.com

[18] G. Ivensky, S. Bronshtein, and A. Abramovitz, "Approximate analysis of resonant LLC DC-DC converter," *IEEE Trans. Power Electron.*, vol. 26, no. 11, pp. 3274–3284, Nov. 2011.

[19] X. Fang, H. Hu, Z. Shen, and I. Batarseh, "Operation mode analysis and peak gain approximation of the LLC resonant converter," *IEEE Trans. Power Electron.*, vol. 27, no. 4, pp. 1985–1995, Apr. 2012.

[20] R. Steigerwald, "A comparison of half-bridge resonant converter topologies," *IEEE Trans. Power Electron.*, vol. 3, no. 2, pp. 174–182, Apr. 1988.

[21] T. Duerbaum, "First harmonic approximation including design constraints," in *Proc. IEEE Int. Conf. Telecommun. Energy*, Oct. 1998, pp. 321–328.

[22] H. Huang, "FHA-Based voltage gain function with harmonic compensation for LLC resonant converter," in *Proc. IEEE 25th Annu. Conf. Appl. Power Electron. Expo.*, Feb. 2010, pp. 1770–1777.

[23] 2nd Generation LLC current resonant control IC FA6A00N Series, [Online]. Available: www.fujielectric.com

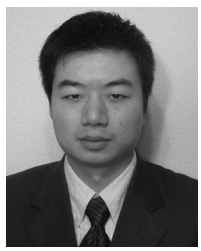

Jian Chen (S'14) was born in China in 1976. He received the B.S. degree from Sun Yat-Sen University, Guangzhou, China, in 1998, and the M.S. degree from Kobe University, Kobe, Japan, in 2007. He is currently working toward the Ph.D. degree in electrical and electronic engineering at Yamanashi University, Yamanashi, Japan.

From 1998 to 2003, he worked with Sumida Corporation, a manufacturer of inductive components, as a Design Engineer. In 2007, he joined Fuji Electric Co., Ltd., Matsumoto, Japan, where he designed power management ICs. He is the holder of 18 U.S. patents. His major research interests include LLC resonant dc–dc converters and PFC boost converters.

Takahide Sato received the Master and Doctor of engineering degree from the Tokyo Institute of Technology, Tokyo, Japan in 2000 and 2005, respectively.

From 2002 to 2009, he was with the Tokyo Institute of Technology, as an Assistant Professor. In 2009, he joined the University of Yamanashi, Japan, where he is currently an Associate Professor. His research interests include analog circuit design, biomedical circuits design, energy harvesting technique, and dc–dc converter design.

Koji Yano (M'01) received the Ph.D. degree from Shizuoka University, Shizuoka, Japan, in 1993.

Since then he joined the Department of Electronics and Computer Science, University of Yamanashi, Japan, as Research Assistant in the fields of design and fabrication processes of power semiconductor devices. From 1999 to 2000, he was a Visiting Researcher in the University of Toronto, Canada. Since 2010, he is a Professor in the University of Yamanashi. Since 2005, he has been engaged in research on power devices of wide bandgap semiconductor materials, especially, SiC and GaN.

Dr. Yano is a member of the Japan Society of Applied Physics and the Institute of Electrical Engineers of Japan.

Hironobu Shiroyama was born in Nagasaki, Japan, in 1967. He received the B.E. and M.E. degrees from Kyushu Univversity, Fukuoka, Japan, in 1990 and 1992, respectively, and the Ph.D. degree in electrical and electronic engineering from the Nagasaki University, Nagasaki, Japan, in 2009.

He is currently with Fuji Electric Co., Ltd. His research interests include power electronics. He is a Member of the IEICE and IEEJ.

Makoto Owa was born in Nagano, Japan, in 1968. He received the B.S. degrees from the Kanazawa Institute of Technology, Ishikawa, Japan, in 1991.

He is currently with Fuji Electric Co., Ltd. His research interests include power electronics.

Masayuki Yamadaya was born in Hokkaido, Japan, in 1971. He received the B.E. and M.E. degrees from Saitama University, Saitama, Japan, in 1993 and 1995, respectively, and the Ph.D. degree in electrical and electronic engineering from the Nagasaki University, Nagasaki, Japan, in 2011.

He joined Fuji Electric Co., Ltd., Matsumoto, Japan, in 1995, where he has been engaged in the development of power management ICs. His current research and development interests include the controllers for converters. He is a member of the IEEJ.